Fatigue of V-notched ZK60 magnesium samples: x-ray damage evolution characterization and failure prediction

Jafar Albinmousa[1]*, Mirco Peron[2], Jobin Jose[3], Ahmed F. Abdelaal[1], Filippo Berto[2]

[1]Mechanical Engineering Department, King Fahd University of Petroleum & Minerals, Dhahran, Saudi Arabia

[2]Department of Mechanical and Industrial Engineering, Norwegian University of Science and Technology, Trondheim, Norway

[3]Center for Engineering Research, King Fahd University of Petroleum & Minerals, Dhahran, Saudi Arabia

* P.O. Box 841 Dhahran, 31261, Saudi Arabia, Phone: +966 (13) 860 1803,

Mobile: +966 50 685 3876, Email: binmousa@kkfupm.edu.sa

*Corresponding author

Highlights

1. V-notched ZK60 specimens were tested under stress-controlled cyclic loading
2. The evolution of crack surface area was analyzed using x-ray tomography
3. Crack surface area of V-notched specimen increases exponentially with cycling
4. SED approach correlates smooth and V-notched specimens within a single band

Abstract

Magnesium and its alloys are very attractive lightweight materials and have a potential of applications in different industries. However, their applications as materials for load bearing components are hindered by the limited knowledge of their fatigue behavior, especially in the presence of notches. The goal of this research is to investigate the fatigue behavior of V-notched specimens machined from ZK60-T5 extruded magnesium. V-notched specimens were loaded at different stress amplitudes. One sample was analyzed using x-ray tomographic to evaluate the damage evolution. In addition, the strain energy density approach was used to analyze fatigue of magnesium for the first time.

Keywords: V-notched specimen; X-ray computed tomography (CT); Crack surface; Strain Energy Density; ZK60 magnesium alloy

1 Introduction

In recent years, magnesium (Mg) and its alloys have gained wide interest in several applications, from biomedical to automotive sector [1–8]. Specifically, their high specific strength renders these materials attractive for load-bearing applications, and automobile parts and different components in aircrafts and helicopters have started being manufactured. However, the diffusion of these materials for structural applications is still limited due to the lack of knowledge regarding their fatigue behavior in presence of geometrical discontinuities (notches). The presence of geometrical discontinuities such as notches is in fact very common in structural components, and they are known to be detrimental for static and fatigue resistance [9–11]. Therefore, being structural parts usually subjected to cyclic loading, a deep

understanding of fatigue damage mechanism of notched Mg alloys, together with the development of a robust design tool for the prediction of the fatigue life of notched components, is fundamental for the widespread diffusion of Mg and its alloys for structural applications. Dealing with the former aspect, analysis of fracture surfaces using scanning electron microscope (SEM) offers tremendous insight about the fracture behavior of the materials. However, in recent years, new techniques, such as X-ray computed tomography (or CT scan), have been developed to provide further and more detailed insights into the fatigue damage evolution. As a non-destructive technique, in fact, x-ray tomography can be used to image with high resolution (around 1 μm) internal features of the materials, such as defects and cracks, continuously during their fatigue evolution. Withers and Preuss [12], for example, showed that X-ray computed tomography can be used to study damage-accumulation mechanisms such as cavitation, fracture, microcracking, fatigue cracking, and stress corrosion cracking in different engineering materials. In addition, Wright et al [13], investigating the damage in aerospace grade carbon fiber–epoxy composites, reported this technique to allow the evaluation of existing damage, and crack initiation and growth models. Dealing with Mg and its alloys, King et al [14] performed in-situ observation of short fatigue crack in cast magnesium Elektron 21 using both X-ray diffraction contrast tomography and microtomography and they were able to map the crack surface length and depth with cycling, reporting the surface length to depth ratio of the crack to be about 1.5. However, further characterizations of the fatigue damage evolution of Mg and its alloys are needed, and this work aims to fulfill this need. To do so, notched ZK60 samples were tested under fatigue and X-ray tomography scans were performed at different intervals to measure the growth of the crack surface with cycling. The choice of the material fell on ZK60 because, among the different Mg alloys, ZK alloys, and specifically ZK60, are particularly interesting for structural materials since the addition of Zinc and Zirconium increase the corrosion resistance

of the base material and the mechanical properties (strength and ductility) due to their grain refinement effect. In addition, this work aims to overcome the other limitation hampering the widespread diffusion of Mg and its alloys in structural applications, i.e. the need of a robust design tool against fatigue in the presence of notches. Several criteria have been developed in the recent years to predict the fatigue behavior of different material classes (metals, ceramics, polymers), from the notch stress intensity factors (NSIFs)-based criterion to the theory of critical distance (TCD) approach [15–18]. However, these criteria suffer of different drawbacks. NSIFs-based criterion, for example, is limited by its geometry dependency and by the need of evaluating accurately the stress field ahead of the geometrical discontinuities to correctly perform the fatigue assessment. The TCD approach, although overcoming the geometry limitation of the NSIFs-based criterion, is still limited by the need to evaluate accurately the stress field. In recent years, the strain energy density (SED) approach has been reported to be a promising candidate for an easy and accurate prediction of the fatigue behavior of different notched materials [19–23] and of real component such as steel rollers [24]. The SED approach, that will be described in detail in Section 3, does not suffer from the geometry dependency and from the need of evaluating accurately the stress field ahead of the geometrical discontinuities, and has therefore gained wide interest among engineers and practitioners, especially for the possibility offered to summarize the fatigue behavior of differently notched components within a single narrow scatter band. However, to the best of the authors' knowledge, the SED approach has never been applied to Mg and its alloys and we thus aim herein to fill this lack. In particular, ZK60 notched specimens were tested under fatigue and the experimental fatigue data were then analyzed in terms of SED.

2 Material & Methodology

2.1 Material

The material used for this investigation is the extruded ZK60-T5 magnesium alloy. This material was acquired from SMW Engineering, Russia, in the form of rods with a diameter of 150 mm and lengths of 1000 mm. The chemical composition of the material is listed in Table 1.

Table 1

Chemical composition (*wt*%) ZK60A-T5.

Mg	Zn	Zr	Others
93.7	5.45	0.58	0.27

The quasi-static behavior of the material was obtained by means of monotonic tensile tests carried out according to ASTM E8-08 standard [25]. The average monotonic tensile properties (elastic modulus, E, yield stress, σ_{ys}, ultimate tensile stress, σ_{UTS}, and elongation to failure, ε_F) of three specimens are listed in Table 2.

Table 2

Monotonic tensile properties of extruded ZK60-T5 magnesium alloy.

$\boldsymbol{E}$ (GPa)	$\boldsymbol{\sigma_{ys}}$ (MPa)	$\boldsymbol{\sigma_{UTS}}$ (MPa)	$\boldsymbol{\varepsilon_F}$ (%)
44.29±0.59	220.7±9.15	284.0±9.9	17.65±1.14

2.2 Microstructure

To observe the microstructure of the material, metallurgical samples were polished in succession using 240, 320, 400 and 600 grit size abrasive papers. Then, the samples were

etched in a solution prepared from 5 g picric acid, 5 ml acetic acid, 10 ml distilled water and 100 ml ethanol [26]. The micrographs were taken using Olympus DSX-CB digital microscope.

2.3 Fatigue Experiment

The V-notch specimens were machined as 16 mm diameter rods with a V-notch that has an opening angle of 60°, a root radius of 0.8 mm and a depth of 1.5 mm as shown in Fig. 1. All samples were cut along the extrusion direction and from the inner part of the rod.

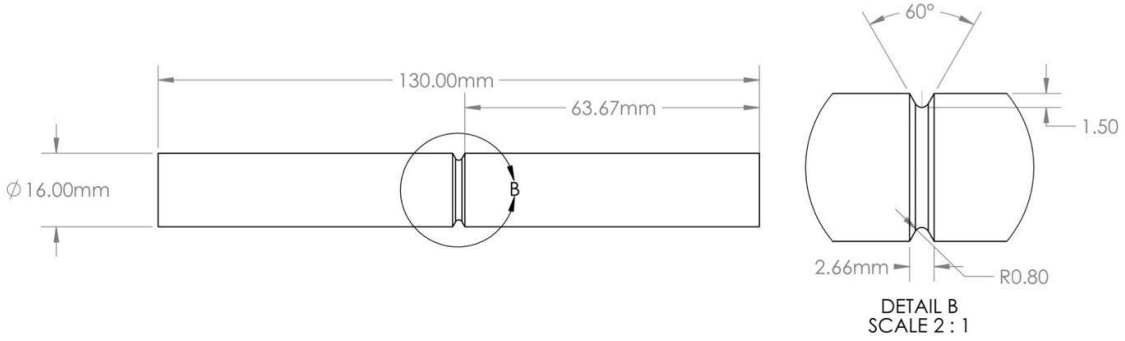

Fig. 1. Geometry and dimensions of V-notch specimen.

Cyclic tests were performed using Instron frame with a loadcell capacity of 100 kN. A total of 17 specimens were tested under fully reversed stress, $R = -1$, uniaxial load-controlled cyclic loading condition and at standard laboratory conditions. Load amplitudes between 9 and 14 kN were applied resulting in a fatigue life range between 17×10^3 and more than 10×10^6 cycles. The fatigue tests were carried out till the complete fracture by separation of the sample into two halves or till the achievement of 13×10^6cycles. Depending on the magnitude of the load amplitude and to make sure that no heating is generated, tests were performed with frequency range between 1 and 30 Hz. The frequency of each test is included in Table 3.

2.4 X-Ray Tomography

The x-ray scans were performed using Nikon XTH 225 ST system. CT scans were performed with energy of 120 kV and a series of 720 radiographs projections were taken to reconstruct the 3D volumes. The total scanning time for each scan was 1.5 hours and a total of 14 scans were taken to assess the crack evolution. The reconstruction and the image processing were done using Inspect-X and Avizo 8.1 software, respectively. Due to the high amount of time required, only one specimen was carefully selected for ex-situ CT-scan analysis, and the following procedure was followed. First, an extensometer was mounted on different specimens that are tested at different amplitudes. The response of the local displacement measured by the extensometer was analyzed. The target was to determine a load amplitude that can initiate a detectable change by the extensometer and before the crack reaches to a critical size. Fig. **2** shows an example of strain measurements recorded with cycling by an extensometer for V-notched specimen loaded with force amplitude of 14 kN. This figure clearly shows that changes in the strain measurement for this load can be detected after 10^4 cycles.

It is worth mentioning that the selected load amplitude shall not be low such that the resulting crack growth period is too long in order to minimize the number of CT-scans. An amplitude of 12 kN was found to be a good choice for this study. Second, two specimens were tested at this amplitude and with the extensometer mounted on them to have an understanding about the fatigue behavior at this load. The resulting fatigue lives from these specimens were between 50×10^3 and 130×10^3 cycles. The third specimen that was tested at this amplitude was targeted to be used for CT-scanning. Hence, the sample was loaded on the

cyclic machine with the extensometer mounted such that the knife-edges are positioned half-way from the V-notch. Fourth, an alignment mark was engraved on the gripping section of the specimen in order to make sure that the specimen is mounted at the same position in the CT-scanner.

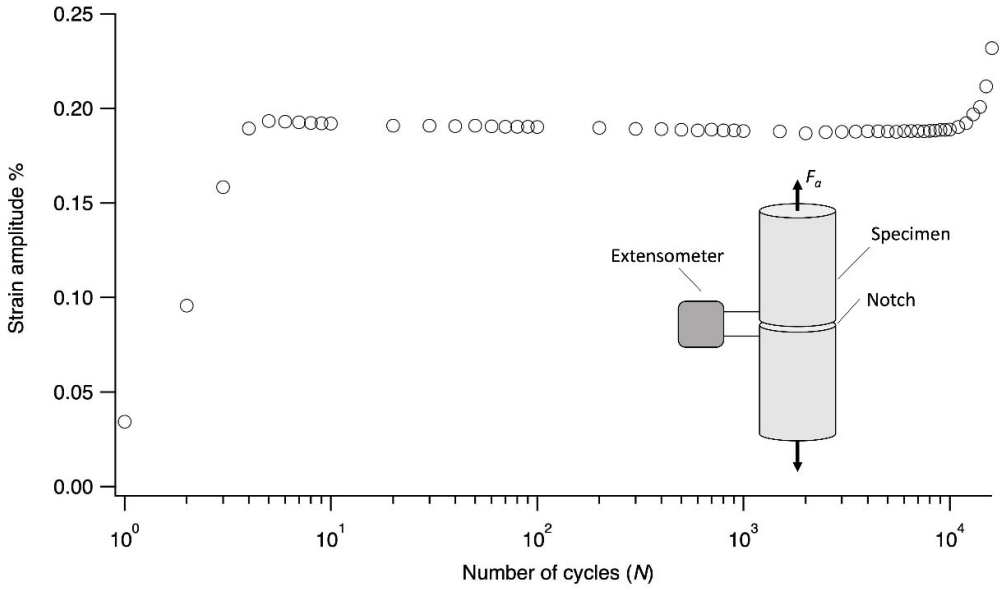

Fig. 2. Strain measurement technique used during stress-controlled cyclic test of V-notched specimen, $F_a = 14$ kN.

A custom-made CT-base was manufactured to fit the size of the specimen and make sure it is secured vertically. This base has an alignment mark also in order to ensure that the sample is always mounted in the same orientation with respect to the x-ray gun and detector. A schematic showing the sample mounted on the CT-base is depicted in Fig. 3. Fifth, from prior knowledge about the behavior of the strain amplitude during the test, the machine is set to stop after a specific change in the strain amplitude. Sixth, the sample is unmounted from the cyclic machine after the stopping criterion is satisfied and is taken to CT-Scan lab. Seventh, the sample is taken again to the cyclic machine to be cycled further. However, no extensometer is mounted at this stage. Rather, depending on the size of the crack imaged by the x-ray scanner the test end-condition is determine by setting a specific number of cycles.

Usually, an increment of 500 to 1000 cycles is defined such that machine is stopped after this specific number of cycles is exhausted. Then, sample is taken again for the next scan. This process is continued until the sample is fractured. Finally, the fractured surfaces are analyzed using scanning-electron microscope as described in the next Section.

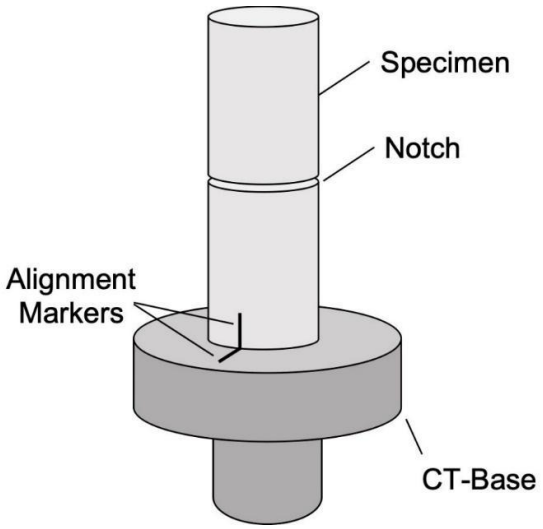

Fig. 3. A schematic illustrating the proper mounting of the sample on the CT-Base using the alignment markers.

2.5 Fracture Surface Analyses

Specimens were cut and prepared for SEM analysis after fatigue failure. Fracture surfaces were analyzed using FEI, Quanta FEG 250 scanning electron microscope. Secondary electron (SE) and back scatter electron (BSE) are used to reveal different fatigue features micro-cracks and striation.

3 Strain Energy Density Approach (SED)

The SED criterion has been proposed and formalized first by Lazzarin and Zambardi [27], where they predict the static and fatigue behavior of different materials weakened by different notch geometries. According to this criterion, the tensile failure of a component

occurs when the total strain energy, $\bar{W}$, averaged in a specific control volume located at a notch or crack tip, reaches the critical value W_c. Now, considering cyclic loadings, when the strain energy range $\Delta\bar{W}$ averaged in a control volume ahead of the notch or crack tip reaches its critical value ΔW_c, the failure will occur. In Ref. [27] a simple analytical formulation for the determination of the critical value of the strain energy density range ΔW_c has been proposed:

$$\Delta W_c = \frac{\Delta\sigma_A^2}{2E} \tag{1}$$

where $\Delta\sigma_A$ is the fatigue limit of the material without geometric singularities and E is the Young's modulus of the material. In plane problems the control volume becomes a circular sector or a circle for V-notches or cracks, respectively (Fig. 4a and b), with the critical radius R_c defined as follow:

$$R_c = \left(\frac{\sqrt{2e_1}\Delta K_{1A}}{\Delta\sigma_A}\right)^{\frac{1}{1-\lambda_1}} \tag{2}$$

where λ_1 is Williams' eigenvalue for mode 1 [28], ΔK_{1A} is the amplitude of the notch stress intensity factors (NSIF) fatigue threshold and e_1 is a parameter dependent on the notch opening angle 2α, on the hypothesis considered (plane strain or plane stress) and on the Poisson's ratio ν (the reader should referred to Ref. [27] for e_1 formulation). In addition, for a blunt V-notch or a U-notch (Fig. 4a or c), the volume is assumed to be of a crescent shape, where R_c is the depth measured along the bisector line. The outer radius of crescent shape is equal to $R_c + r_0$, being r_0 the distance between the notch tip and the origin of the local coordinate system (Fig. 4c). Such a distance depends on the notch opening angle 2α, according to the expression:

$$r_0 = \rho\frac{(\pi-2\alpha)}{(2\pi-2\alpha)} \tag{3}$$

Berto et al. [30] analyzed the fatigue behavior of innovative alloys at high temperature and, using Ansys® code, they obtained the critical radius value varying the control volume until the SED value for a notched specimen at a certain amount of cycles matches the critical SED value obtained for a plain specimen failed at the same number of cycles (Eq. (1)). In this work, the NSIF fatigue threshold is un-known, and thus the critical values are obtained using a similar approach to that in Ref. [30]. The critical radius has been determined as the value at which the SED values for two different specimen geometries at the same number of cycles are equal. Moreover, this SED value has been considered as the critical one. A deeper explanation will be provided in the next section.

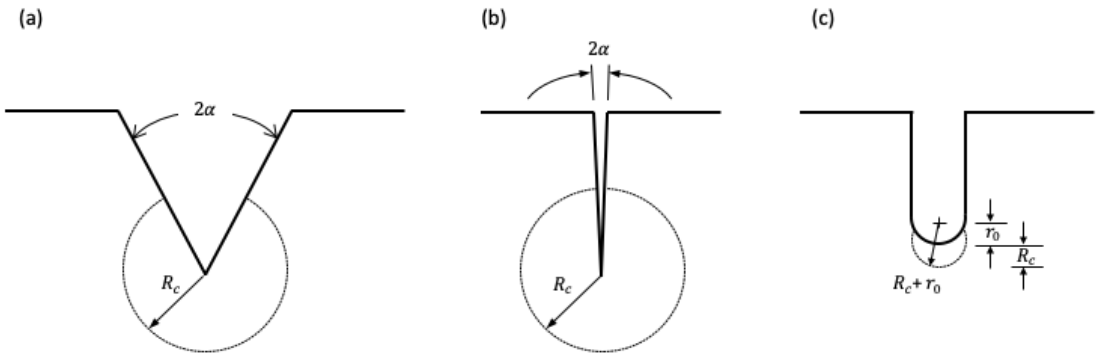

Fig. 4. Control volume for sharp V-notch (a), crack case (b) and U notch (c) under mode I loading.

4 Finite Element Analysis

In order to obtain the SED value, axisymmetric linear elastic 2D analyses were performed on the notched models. Due to the double symmetry of the geometry, only one quarter of the specimens were modeled. The 8-nodes axisymmetric element plane 83 was selected for these analyses. The element size at the crack tip of 2.91×10^{-3} mm^2. Symmetric boundary conditions were used for vertical and horizontal symmetry lines of the models; however, the

top side of the model was able to move along the loading axis (Fig. 5). Being the NSIF fatigue threshold not available, Eq. (2) cannot be applied to determine the critical radius, and the alternative approach proposed by Berto et al. [30] was used as followed.

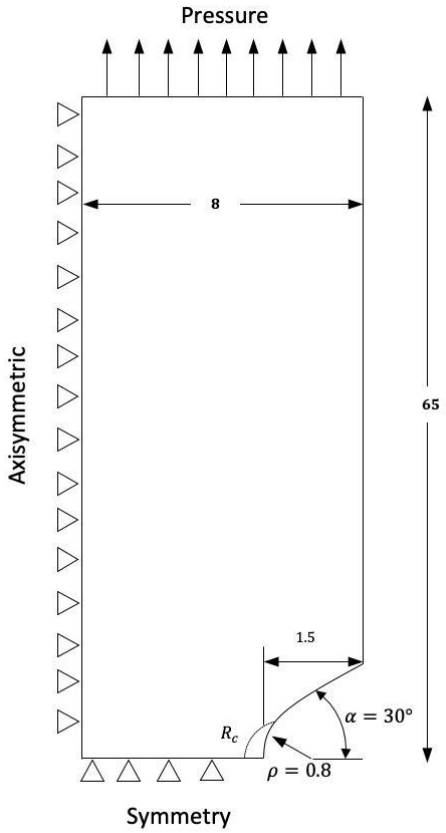

Fig. 5. Finite element geometry, load ad boundary conditions of V-notched specimen. Dimensions in mm.

First, the reference cycle was considered as 10^6 and an average load of 10.8 kN was applied as listed in Table 3 in the next Section. This load results in an average applied stress of 53 MPa on the gripping section of the specimen. Therefore, the critical radius is estimated by applying a stress range of 106 MPa and calculating the resulting strain energy density in the critical region. Then, the obtained strain energy density from finite element analysis is compared with that obtained from Eq. (1) for un-notched specimen. This equation requires

the determination of the applied normal stress range on an un-notched specimen machined from the same alloy that resulted in a fatigue life of 10^6 cycles. Pahlevanpour et al [31,32] performed stress- and strain-controlled fatigue experiments on ZK60 extrusion. Albinmousa et al [33] performed strain-controlled fatigue experiment on the alloy investigated here. Because the strain-life curve of Pahlevanpour et al [31,32] is significantly similar to that of Albinmousa et al [33], the stress-life curve of Pahlevanpour et al [31,32] was used to determine the average stress range that can be applied on an un-notched specimen and result in a fatigue life of 10^6 cycles. This stress range was found to be 244.4 MPa which yields $\Delta W_c = 0.67$ MJ/m^3. ANSYS APDL code was used to perform parametric analysis by applying pressure boundary condition of 106 MPa and changing the radius R_c until the resulting strain energy density in the control volume is equal to $\Delta W_c = 0.67$ MJ/m^3. The obtained radius was $R_c = 0.42$ mm. The average strain energy in the control volume is shown in Fig. 6. Because the radius of the control volume is a material property, the same value of R_c is used to obtain the strain energy density for the remaining specimens listed in Table 3 by applying the corresponding stress range for each specimen.

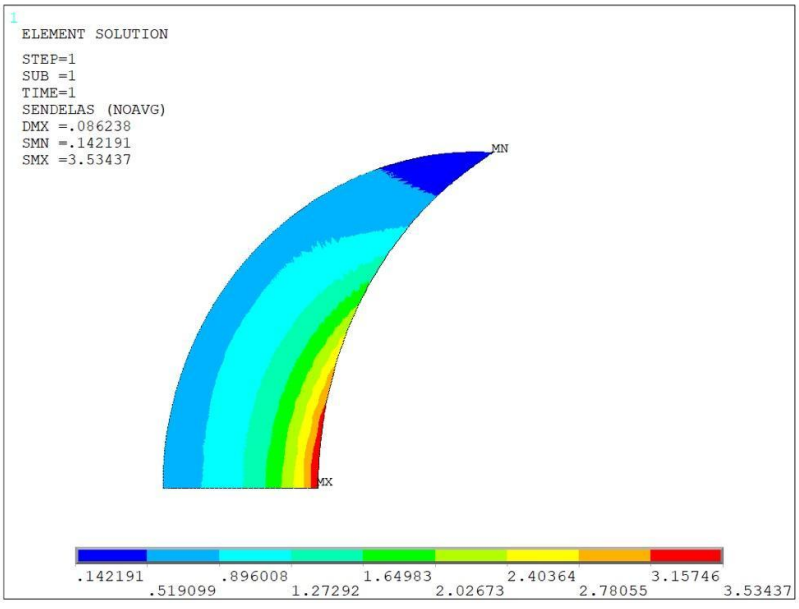

Fig. 6. Elastic strain energy in the control volume. Applied pressure is 140 MPa and $R_c = 0.42$ mm.

5 Results and Discussion

5.1 Microstructure

Fig. **7** shows the microstructure of ZK60A-T5 along the extrusion direction which is made up of a combination of large and small grains with an average grain size of 9.52 ± 1.89 μm. The texture measurement of the material was performed at the Fatigue and Stress Analysis Lab in the University of Waterloo, Canada. A Bruker D8 Discover X-ray diffractometer equipped with an advanced 2D-detector using CuKα beam radiation at the voltage of 40 kV and current of 40 mA was used. The pole figures plot in Fig. 8 show that the majority basal planes are parallel to the extrusion direction. This texture is commonly observed in other magnesium extrusions such as AZ80 [34,35], AZ61 [36], AZ31 [37–40], AM30 [41] and in ZK60 investigated by other researchers [42,43].

Fig. 7. Microstructure of ZK60A-T5 in the extrusion direction.

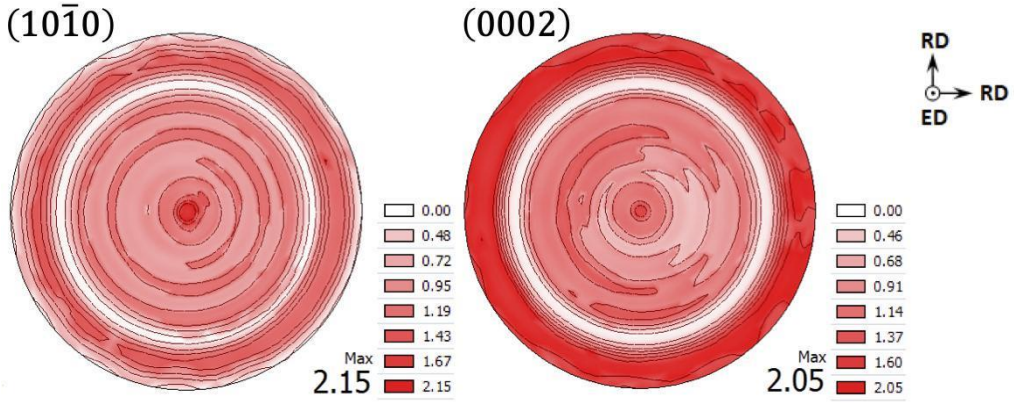

Fig. 8. (10$\bar{1}$0) and (0002) pole figures for ZK60A-T5 magnesium extrusion.

5.2 Fatigue Experiment

All the fatigue experiments on the notched ZK60-T5 extruded alloy are reported in Table 3 and in Fig. 9, where the results for the un-notched specimens tested by Pahlevanpour et al [31,32] are also reported, clearly showing the detrimental effect of the notch on fatigue strength of the material. It is worth mentioning that the sample HCF-ZK60-V20 is that used for ex-situ x-ray characterizations.

Table 3

Summary of fatigue test on V-notch ZK60 samples. F_a: force amplitude and σ_{nom} : nominal stress (calculated at the gripping section).

No.	Specimen ID	Freq (Hz)	F_a (kN)	σ_{nom} (MPa)	N_f (Cycles)
1.	HCF-ZK60-V02	1.0	14.0	105.5	17,203
2.	HCF-ZK60-V18	1.0	14.0	105.5	18,243
3.	HCF-ZK60-V17	1.0	14.0	105.5	19,703
4.	HCF-ZK60-V12	1.5	14.0	105.5	20,509
5.	HCF-ZK60-V16	1.0	14.0	105.5	28,879

6.	HCF-ZK60-V01	1.0	12.0	90.4	52,479
7.	HCF-ZK60-V19	4.0	12.0	90.4	136,330
8.	HCF-ZK60-V20*	4.0	12.0	90.4	184,005
9.	HCF-ZK60-V05	8.0	11.0	82.9	239,733
10.	HCF-ZK60-V11	4.0	12.0	90.4	324,649
11.	HCF-ZK60-V10	20.0	11.0	82.9	1,114,854
12.	HCF-ZK60-V07	15.0	10.5	79.1	1,144,682
13.	HCF-ZK60-V13	15.0	10.5	79.1	1,713,655
14.	HCF-ZK60-V04	10.0	10.0	75.3	4,274,061
15.	HCF-ZK60-V09	30.0	9.5	71.6	6,634,977
16.	HCF-ZK60-V03	15.0	9.0	67.8	10,088,009
17.	HCF-ZK60-V08	30.0	9.0	67.8	13,159,564→

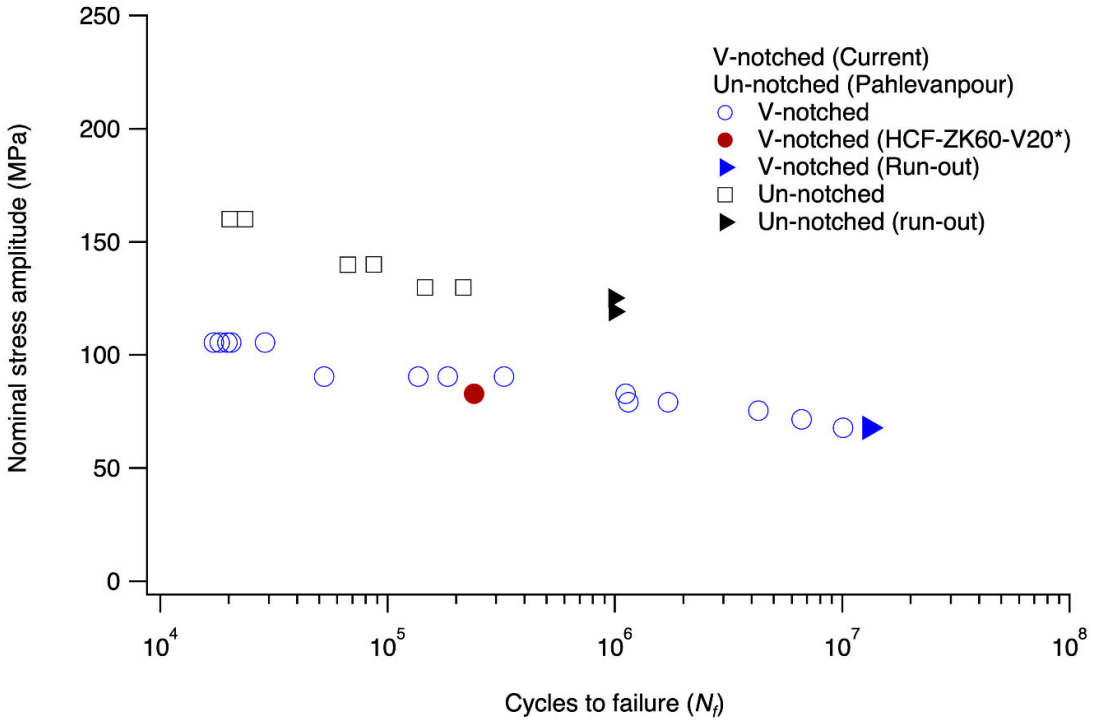

Fig. 9. Nominal stress life curve. Un-notched are from Refs [31,32].

5.3 X-Ray Tomography

Specimen HCF-ZK60-V20* was successfully used for ex-situ x-ray tomography. Therefore, the test on this specimen was interrupted 15 times for x-ray imaging. After reconstruction, the volume surrounding the notch was sliced into nearly 250 layers. The thickness of each slice is nearly 10.72 μm. After that, the layers that does not have crack features are eliminated. Then, the layers that have crack features are segmented using gray-level thresholding process. A single threshold value is used in the whole image depending on the CT scan image histogram. The gray-level thresholding process is assigned to each pixel to convert it to white or black pixel using MATLAB such that white and black are assigned to the background area and the crack area, respectively. Finally, a photo editing software is used to extract the crack area from each layer and merge all crack layers into one image. As a result, the final image represents the actual projected area of the crack surface as shown in Fig. 10.

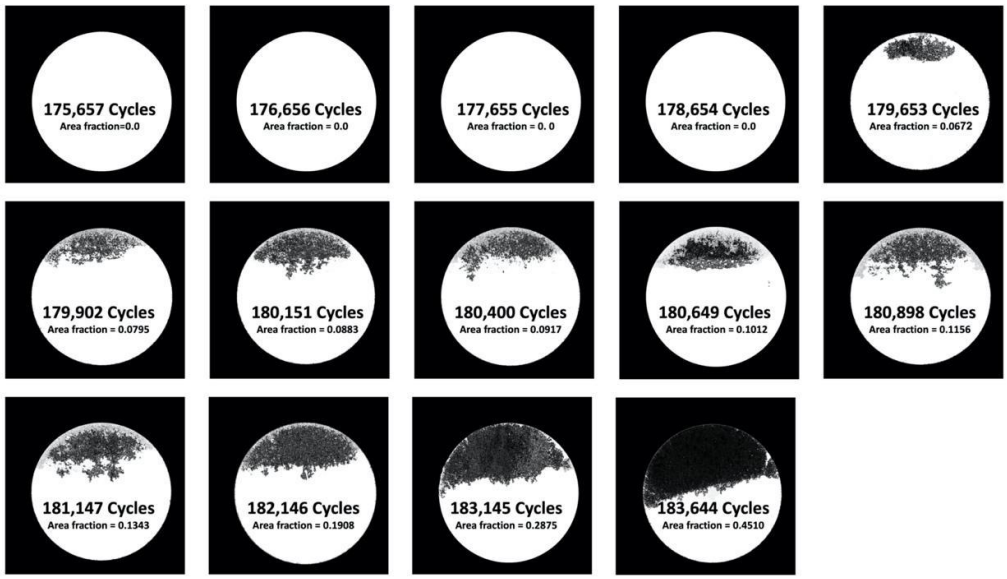

Fig. 10. Area fraction of projected crack surface obtained using x-ray tomography for sample HCF-ZK60-V20*. F_a = 12 kN and N_f = 184,005 cycles.

Fig. **11**A shows a slice that demonstrates part of the surface morphology of the crack. A close examination of all slices shows that the crack grew within 30 slices. Because thickness of each slice is nearly 10.72 μm, it can be estimated that the absolute crack height, i.e., from valley to peak, is 322 μm. Yet, a 3D segmentation of the crack surface shown in Fig. 11B clearly reveals that the crack can be idealized as 2D geometry. A sequence of slices in graphics interchange format is included as a supplementary material to display the crack surface at different height.

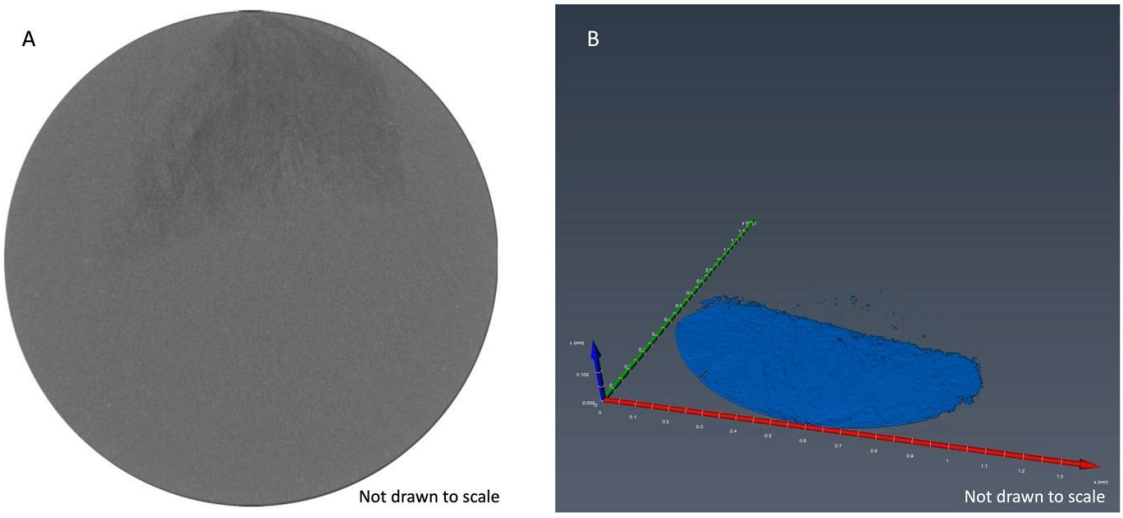

Fig. 11. Reconstruction of x-ray scans. (A) A slice at V-notch showing part of crack surface. (B) A 3D visualization of the crack surface.

A major objective of this investigation is the calculation of crack size as a function of loading cycles. Using the results shown in Fig. 10 and assuming that fatigue crack is a flat surface that grew at the root of the v-notch, the actual projected crack area can be estimated and represented as function of loading cycles as shown in Fig. 12. It is important to note that the

measurements between 175,657 and 178,654 cycles shown in Fig. 10 should not infer that there is no physical crack. Rather, we think that capturing smaller crack would require more advance technique and/or facility such as micro-computed tomography. A close examination of this figure suggests an exponential relation between the actual project crack area and number of cycles. The fitting parameters for exponential fit, Eq. (4), obtained using MATLAB are $\kappa = 2.4 \times 10^{-31}\text{mm}^2$ and $\eta = 4.05 \times 10^{-4}$ with goodness of fit $R^2 = 0.9923$.

$$A_p = \kappa e^{\eta N} \tag{4}$$

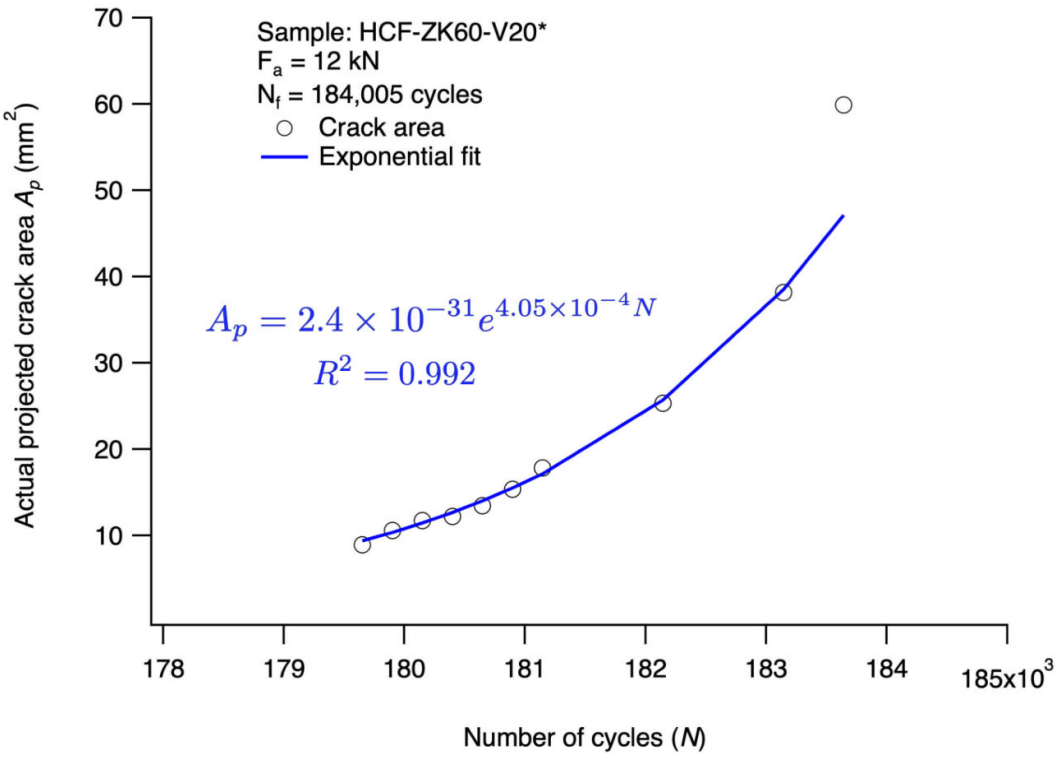

Fig. 12. Exponential correlation between projected crack area and number of cycles for V-notched specimen subjected fully reversed cyclic axial loading.

5.4 Fractography Analysis

Fatigue damage mechanisms of magnesium alloys are still under investigations. There are three major observations reported in the literature. The first suggests that fatigue crack initiation is related to intermetallic particles that are widely observed in wrought magnesium alloys [36,44]. The second suggests that fatigue crack initiation is related to persistent slip bands (PSB) [45–47] and/or twinning-detwinning deformation [48]. The third suggests that fatigue crack initiation is related to twin-slip interaction [49]. Fatigue surface of specimen HCF-ZK60-V20* was examined using SEM. Fatigue crack propagation site is characterized by striation feature and secondary cracks as shown in Fig. 13. Multiple micro-cracks were observed and measured. The sizes of these micro-cracks range between $4.8\,\mu$m to $16.6\,\mu$m with an average size of $10.26 \pm 4.3\,\mu$m. On the other hand, the average distance between each striation is $1.46 \pm 0.79\,\mu$m. Several secondary phase particles were observed in the matrix with an average size of $5.18 \pm 2.11\,\mu$m. In addition, dimple-like ductile fracture features and tear ridges are observed. Based on these observations, it is possible that fatigue damage mechanism is controlled by the initiation of micro-cracks around intermetallic particles. These cracks are likely to coalesce into a domain crack that leads to final failure. that The transition region between the crack growth and the final rupture is characterized by shallow dimples and its surface is rather rough as shown in Fig. 14.

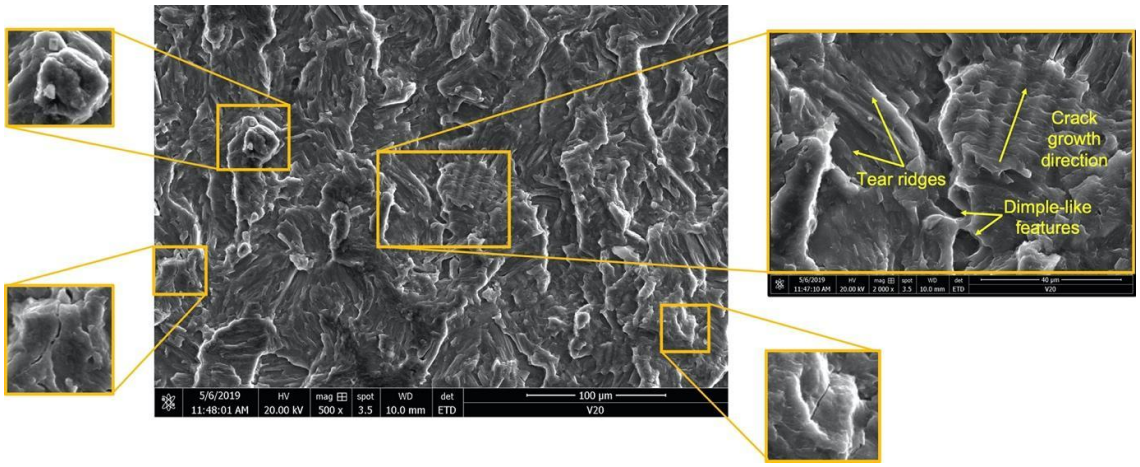

Fig. 13. Crack propagation site showing dimple-like features, tear ridges, microcracks and second phase particles.

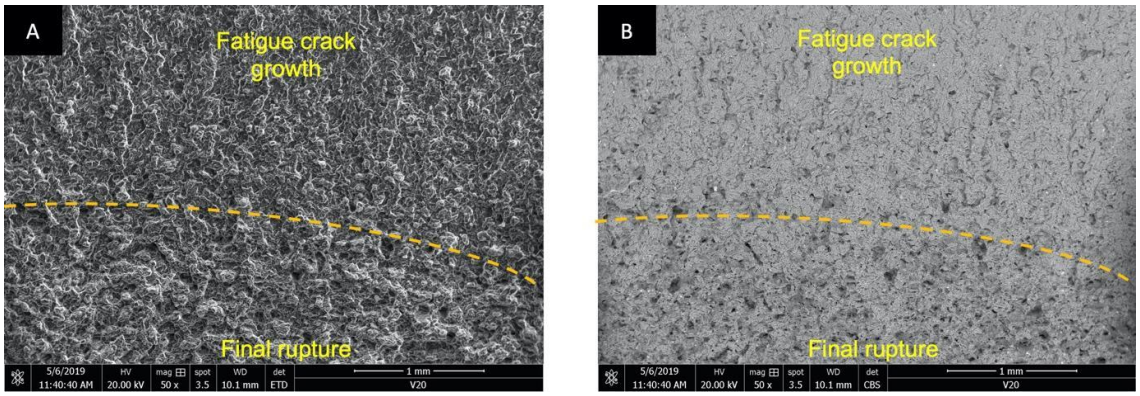

Fig. 14. Transition region between fatigue crack growth and final rupture. (A) Secondary electron (SE) and (B) Back scatter electron (BSE).

5.5 Strain Energy Density

Once the critical radius was determined as reported in Section 4, the experimental fatigue data reported in Table 3 and the experimental data obtained by Pahlevanpour et al [31,32] for un-notched samples were analyzed in terms of SED range. FE analyses were carried out considering the experimental stress range as the applied load in the simulations, determining the corresponding SED range value used to obtain the fatigue curve shown in Fig. 15.

The fatigue results for notched and un-notched extruded ZK60-T5 samples fall within a single narrow scatter band, with an inverse slope k = 6.83 and a strain energy density range referred to 2 million loading cycles and to a probability of survival of 50% of 0.60 MJ/m^3 In fact, the scatter index T_W, related to the two curves with probabilities of survival Ps = 2.3% and 97.7%, is 1.257. T_W =1.257 becomes equal to 1.12 when reconverted to an equivalent local stress range being the SED proportional to the square of the stress.

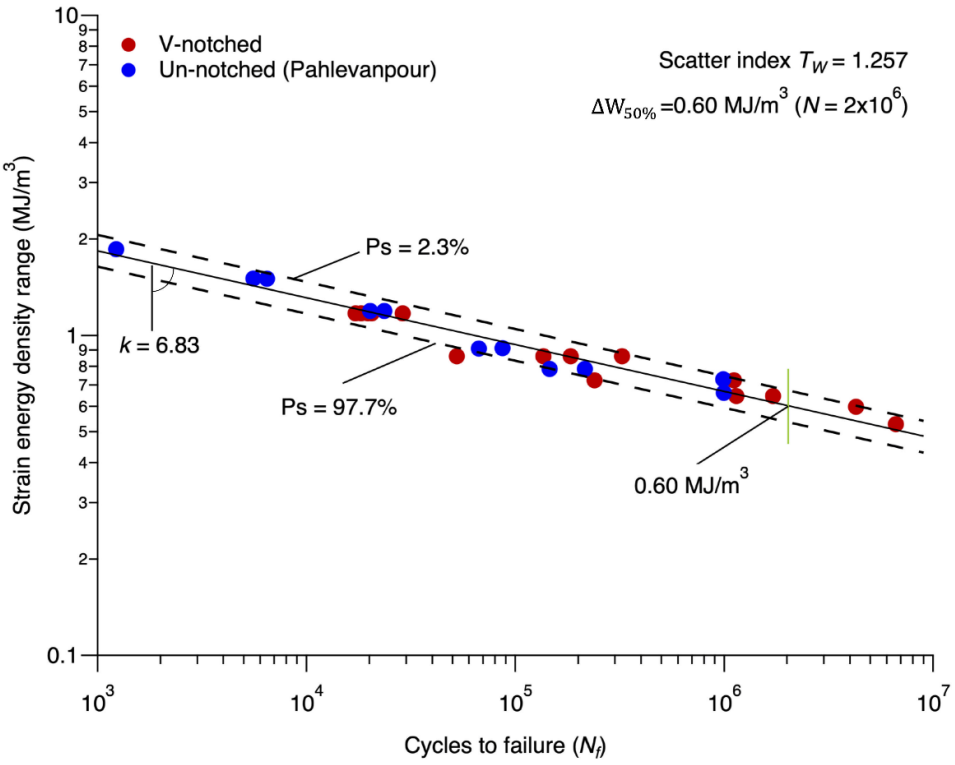

Fig. 15. Correlation between strain energy density and fatigue life for un-notched (smooth) [31,32] and V-notched specimens.

6 Conclusion

In this work, new insights into the fatigue behavior of ZK60-T5 extruded Mg alloy were provided. V-notched specimens machined from ZK60 magnesium extrusion were tested under stress-controlled cyclic axial loading. One selectede sample was used for ex-situ x-ray

tomographic analysis. Fatigue test was interrupted 14 time to conduct CT scans on this sample. After segmentations analysis of the x-ray images, the crack surface areas at different cycles were revealed. The obtained results suggest that the crack surface area an exponentially related to the number of cycles. In addition, the applicability of SED approach as a tool to provide a unique master curve for ZK60 magnesium samples with different geometries was assessed for the first time. The results are promising as they show that the experimental fatigue data obtained here for ZK60 notched samples and the fatigue data reported in literature for smooth samples fall within a single narrow scatter band.

Acknowledgement

The authors would like to acknowledge the supported of King Fahd University of Petroleum & Minerals (KFUPM) for supporting this work under Internal Funded Grant, Project No. IN161044.

Author statement

Jafar Albinmousa: Funding acquisition, Project administration, Supervision, Writing Review & Editing, Conceptualization, Formal analysis.

Jobin Jose: Data Curation, Resources.

Ahmed F. Abdelaal: Visualization, Software.

Mirco Peron: Software, Formal analysis, Writing Review & Editing

Filippo Berto: Writing Review & Editing

Data availability statement

The raw data required to reproduce these findings are available to download from Mendeley Data:
Albinmousa, Jafar (2019), "Fatigue Crack Imaging of V-Notched Specimen using X-Ray Tomography", Mendeley Data, v1 http://dx.doi.org/10.17632/sdgpv9ccv2.1

References

[1] Albinmousa J, Pascu A, Jahed H, Horstemeyer MF, Luo A, Chen D, et al. Monotonic and Fatigue Behavior of Magnesium Extrusion Alloy AM30: An International Benchmark Test in the "Magnesium Front End Research and Development Project," SAE International; 2010. https://doi.org/10.4271/2010-01-0407.

[2] Forsmark JH, Li M, Su X, Wagner DA, Zindel J, Luo AA, et al. The USAMP Magnesium Front End Research and Development Project — Results of the Magnesium "Demonstration" Structure. In: Alderman M, Manuel MV, Hort N, Neelameggham NR, editors. Magnesium Technology 2014, Cham: Springer International Publishing; 2016, p. 517–24. https://doi.org/10.1007/978-3-319-48231-6_93.

[3] Luo AA, Nyberg EA, Sadayappan K, Shi W. Magnesium Front End Research and Development: A Canada-China-USA Collaboration. In: Mathaudhu SN, Luo AA, Neelameggham NR, Nyberg EA, Sillekens WH, editors. Essential Readings in Magnesium Technology, Cham: Springer International Publishing; 2016, p. 41–8. https://doi.org/10.1007/978-3-319-48099-2_6.

[4] Aghion E, Bronfin B. Magnesium Alloys Development towards the 21st Century. MSF 2000;350–351:19–30. https://doi.org/10.4028/www.scientific.net/MSF.350-351.19.

[5] Albinmousa J. Fatigue of Magnesium-Based Materials. Magnesium-The Wonder Element for Engineering/Biomedical Applications, IntechOpen; 2020.

[6] Peron M, Bertolini R, Ghiotti A, Torgersen J, Bruschi S, Berto F. Enhancement of stress corrosion cracking of AZ31 magnesium alloy in simulated body fluid thanks to cryogenic machining. Journal of the Mechanical Behavior of Biomedical Materials 2020;101:103429. https://doi.org/10.1016/j.jmbbm.2019.103429.

[7] Peron M, Torgersen J, Berto F. Mg and Its Alloys for Biomedical Applications: Exploring Corrosion and Its Interplay with Mechanical Failure. Metals 2017;7:252–252. https://doi.org/10.3390/met7070252.

[8] Mathaudhu SN, Nyberg EA. Magnesium Alloys in U.S. Military Applications: Past, Current and Future Solutions. In: Mathaudhu SN, Luo AA, Neelameggham NR, Nyberg EA, Sillekens WH, editors. Essential Readings in Magnesium Technology, Cham: Springer International Publishing; 2016, p. 71–6. https://doi.org/10.1007/978-3-319-48099-2_10.

[9] Cicero S, Torabi AR, Madrazo V, Azizi P. Prediction of fracture loads in PMMA U-notched specimens using the equivalent material concept and the theory of critical distances combined criterion. Fatigue & Fracture of Engineering Materials & Structures 2018;41:688–699.

[10] Wang QG, Apelian D, Lados DA. Fatigue behavior of A356-T6 aluminum cast alloys. Part I. Effect of casting defects. Journal of Light Metals 2001;1:73–84.
[11] Seweryn A, Poskrobko S, Mróz Z. Brittle fracture in plane elements with sharp notches under mixed-mode loading. Journal of Engineering Mechanics 1997;123:535–543.
[12] Withers PJ, Preuss M. Fatigue and damage in structural materials studied by X-ray tomography. Annual Review of Materials Research 2012;42:81–103.
[13] Wright P, Moffat A, Sinclair I, Spearing SM. High resolution tomographic imaging and modelling of notch tip damage in a laminated composite. Composites Science and Technology 2010;70:1444–52. https://doi.org/10.1016/j.compscitech.2010.04.012.
[14] King A, Ludwig W, Herbig M, Buffire JY, Khan AA, Stevens N, et al. Three-dimensional in situ observations of short fatigue crack growth in magnesium. Acta Materialia 2011;59:6761–71. https://doi.org/10.1016/j.actamat.2011.07.034.
[15] Verreman Y, Nie B. EARLY DEVELOPMENT OF FATIGUE CRACKING AT MANUAL FILLET WELDS. Fat Frac Eng Mat Struct 1996;19:669–81. https://doi.org/10.1111/j.1460-2695.1996.tb01312.x.
[16] Lazzarin P, Tovo R. A NOTCH INTENSITY FACTOR APPROACH TO THE STRESS ANALYSIS OF WELDS. Fat Frac Eng Mat Struct 1998;21:1089–103. https://doi.org/10.1046/j.1460-2695.1998.00097.x.
[17] Kasiri S, Taylor D. A critical distance study of stress concentrations in bone. Journal of Biomechanics 2008;41:603–9. https://doi.org/10.1016/j.jbiomech.2007.10.003.
[18] Prawoto Y. Application of linear elastic fracture mechanics in materials science and engineering: easy and simple guide to use fracture mechanics outside the mechanics world. Morrisville, NC: Lulu Enterprises; 2011.
[19] Campagnolo A, Razavi SMJ, Peron M, Torgersen J, Berto F. Mode II brittle fracture: Recent developments. Frattura Ed Integrità Strutturale 2017;11:181–188.
[20] Razavi SMJ, Peron M, Torgersen J, Berto F. Notched graphite under multiaxial loading. Frattura Ed Integrit‡ Strutturale 2017;11:424–431.
[21] Peron M, Razavi SMJ, Berto F, Torgersen J. Notch stress intensity factors under mixed mode loadings: an overview of recent advanced methods for rapid calculation 2017.
[22] Peron M, Razavi SMJ, Berto F, Torgersen J, Mutignani F. Local strain energy density for the fatigue assessment of hot dip galvanized welded joints: Some recent outcomes 2017.
[23] Razavi SMJ, Peron M, Mutignani F, Torgersen J, Berto F. Fatigue strength of hot-dip galvanized welded steel connections. Key Engineering Materials, vol. 754, Trans Tech Publ; 2017, p. 244–247.
[24] Chebat F, Peron M, Viespoli LM, Welo T, Berto F. Fatigue strength assessment of steel rollers: on the reliability of the strain energy density approach on real components. Applied Sciences 2018;8:1015.
[25] ASTM International. ASTM E8 / E8M-16a, Standard Test Methods for Tension Testing of Metallic Materials 2016. https://doi.org/10.1520/E0008_E0008M-16A.
[26] Hadadzadeh A, Wells MA, Shaha SK, Jahed H, Williams BW. Role of compression direction on recrystallization behavior and texture evolution during hot deformation of extruded ZK60 magnesium alloy. Journal of Alloys and Compounds 2017;702:274–89. https://doi.org/10.1016/j.jallcom.2017.01.236.
[27] Lazzarin P, Zambardi R. A finite-volume-energy based approach to predict the static and fatigue behavior of components with sharp V-shaped notches. International Journal of Fracture 2001;112:275–98. https://doi.org/10.1023/A:1013595930617.
[28] Williams ML. Stress singularities resulting from various boundary conditions in angular corners on plates in extension. Journal of Applied Mechanics 1952;19:526–8.

[29] Berto F, Lazzarin P. Recent developments in brittle and quasi-brittle failure assessment of engineering materials by means of local approaches. Materials Science & Engineering R 2014;75:1–48. https://doi.org/10.1016/j.mser.2013.11.001.
[30] Berto F, Gallo P, Razavi SMJ, Ayatollahi MR. Fatigue behavior of innovative alloys at elevated temperature. Procedia Structural Integrity 2017;3:162–7. https://doi.org/10.1016/j.prostr.2017.04.029.
[31] Pahlevanpour A. Role of Loading Direction on Fatigue Behavior of Smooth and Notched ZK60 Extrusion. UWSpace, 2018.
[32] Pahlevanpour AH, Karparvarfard SMH, Shaha SK, Behravesh SB, Adibnazari S, Jahed H. Anisotropy in the quasi-static and cyclic behavior of ZK60 extrusion: Characterization and fatigue modeling. Materials & Design 2018;160:936–48. https://doi.org/10.1016/j.matdes.2018.10.026.
[33] Albinmousa J, Adinoyi MJ, Merah N. Multiaxial fatigue of extruded ZK60 magnesium alloy. Fatigue and Fracture of Engineering Materials and Structures 2019. https://doi.org/10.1111/ffe.13048.
[34] Xiong Y, Jiang Y. Cyclic deformation and fatigue of rolled AZ80 magnesium alloy along different material orientations. Materials Science and Engineering A 2016;677:58–67. https://doi.org/10.1016/j.msea.2016.09.031.
[35] Gryguć A, Behravesh SB, Shaha SK, Jahed H, Wells M, Williams B, et al. Multiaxial cyclic behaviour of extruded and forged AZ80 Mg alloy. International Journal of Fatigue 2019;127:324–37. https://doi.org/10.1016/j.ijfatigue.2019.06.015.
[36] Jordon JB, Gibson JB, Horstemeyer MF, El Kadiri H, Baird JC, Luo AA. Effect of twinning, slip, and inclusions on the fatigue anisotropy of extrusion-textured AZ61 magnesium alloy. Materials Science and Engineering A 2011;528:6860–71. https://doi.org/10.1016/j.msea.2011.05.047.
[37] Zheng S, Yu Q, Jiang Y. An experimental study of fatigue crack propagation in extruded AZ31B magnesium alloy. International Journal of Fatigue 2013;47:174–83. https://doi.org/10.1016/j.ijfatigue.2012.08.010.
[38] Xiong Y, Yu Q, Jiang Y. Multiaxial fatigue of extruded AZ31B magnesium alloy. Materials Science and Engineering: A 2012;546:119–28. https://doi.org/10.1016/j.msea.2012.03.039.
[39] Wang Y, Culbertson D, Jiang Y. An experimental study of anisotropic fatigue behavior of rolled AZ31B magnesium alloy. Materials & Design 2019:108266. https://doi.org/10.1016/j.matdes.2019.108266.
[40] Al Bin Mousa J. Multiaxial Fatigue Characterization and Modeling of AZ31B Magnesium Extrusion. University of Waterloo, 2011.
[41] Roostaei AA, Jahed H. Role of loading direction on cyclic behaviour characteristics of AM30 extrusion and its fatigue damage modelling. Materials Science and Engineering A 2016;670:26–40. https://doi.org/10.1016/j.msea.2016.05.116.
[42] Xiong Y, Yu Q, Jiang Y. An experimental study of cyclic plastic deformation of extruded ZK60 magnesium alloy under uniaxial loading at room temperature. International Journal of Plasticity 2014;53:107–24. https://doi.org/10.1016/j.ijplas.2013.07.008.
[43] Karparvarfard SMH, Shaha SK, Behravesh SB, Jahed H, Williams BW. Fatigue characteristics and modeling of cast and cast-forged ZK60 magnesium alloy. International Journal of Fatigue 2019;118:282–97. https://doi.org/10.1016/j.ijfatigue.2018.03.019.
[44] Bernard JD, Jordon JB, Horstemeyer MF, Kadiri HE, Baird J, Lamb D, et al. Structure–property relations of cyclic damage in a wrought magnesium alloy. Scripta Materialia 2010;63:751–6. https://doi.org/10.1016/j.scriptamat.2010.05.048.

[45] Gall K, Biallas G, Maier HJ, Gullett P, Horstemeyer MF, McDowell DL. In-situ observations of low-cycle fatigue damage in cast AM60B magnesium in an environmental scanning electron microscope. Metall and Mat Trans A 2004;35:321–31. https://doi.org/10.1007/s11661-004-0133-5.
[46] Gall K, Biallas G, Maier HJ, Gullett P, Horstemeyer MF, McDowell DL, et al. In-situ observations of high cycle fatigue mechanisms in cast AM60B magnesium in vacuum and water vapor environments. International Journal of Fatigue 2004;26:59–70. https://doi.org/10.1016/S0142-1123(03)00079-3.
[47] Gall K, Biallas G, Maier HJ, Horstemeyer MF, McDowell DL. Environmentally influenced microstructurally small fatigue crack growth in cast magnesium. Materials Science and Engineering: A 2005;396:143–54. https://doi.org/10.1016/j.msea.2005.01.014.
[48] El Kadiri H, Oppedal AL. A crystal plasticity theory for latent hardening by glide twinning through dislocation transmutation and twin accommodation effects. Journal of the Mechanics and Physics of Solids 2010;58:613–24. https://doi.org/10.1016/j.jmps.2009.12.004.
[49] Koike J, Fujiyama N, Ando D, Sutou Y. Roles of deformation twinning and dislocation slip in the fatigue failure mechanism of AZ31 Mg alloys. Scripta Materialia 2010;63:747–50. https://doi.org/10.1016/j.scriptamat.2010.03.021.